

# VARIABLE AND POLARIZED RADIO EMISSION FROM THE T6 BROWN DWARF WISEP J112254.73+255021.5

P. K. G. WILLIAMS<sup>1</sup>, J. E. GIZIS<sup>2</sup>, E. BERGER<sup>1</sup>

<sup>1</sup>Harvard-Smithsonian Center for Astrophysics, 60 Garden Street, Cambridge, MA 02138, USA

<sup>2</sup>Department of Physics and Astronomy, University of Delaware, Newark, DE 19716, USA

## ABSTRACT

Route & Wolszczan (2016) recently detected five radio bursts from the T6 dwarf WISEP J112254.73+255021.5 and used the timing of these events to propose that this object rotates with an ultra-short period of  $\sim 17.3$  minutes. We conducted follow-up observations with the Very Large Array and Gemini-North but found no evidence for this periodicity. We do, however, observe variable, highly circularly polarized radio emission possibly with a period of 116 minutes, although our observation lasted only 162 minutes and so more data are needed to confirm it. Our proposed periodicity is typical of other radio-active ultracool dwarfs. The handedness of the circular polarization alternates with time and there is no evidence for any unpolarized emission component, the first time such a phenomenology has been observed in radio studies of very low-mass stars and brown dwarfs. We suggest that the object’s magnetic dipole axis may be highly misaligned relative to its rotation axis.

**Keywords:** brown dwarfs — radio continuum: stars — stars: individual (WISEP J112254.73+255021.5)

## 1. INTRODUCTION

It has long been recognized that some M dwarf stars vary both spectroscopically and photometrically (Luyten 1926; van Maanen 1940). Early on, theorists concluded that despite their small sizes, these stars must harbor magnetic field more powerful than those of the Sun (*e.g.*, Schatzman 1967), although this hypothesis was not confirmed until the pioneering observations of Saar & Linsky (1985). While theoretical considerations drove the assumption that the coolest M dwarfs would not be able to generate magnetic fields as strong as those of the classical flare stars (*e.g.*, Durney et al. 1993), radio observations have demonstrated that strong dynamo action extends not only to more massive brown dwarfs (Berger et al. 2001) but even to the T dwarfs, which have effective temperatures of just  $\approx 1000$  K (Route & Wolszczan 2012, 2016; Kao et al. 2016). Evidently the loss of the “tachocline” — the shearing layer between the radiative core and convective outer envelope that is argued to be important to the solar dynamo (Ossendrijver 2003, and references therein) — does not preclude the generation of strong magnetic fields in these objects, which are fully convective.

There is nonetheless ample evidence that the magnetic properties of the ultracool dwarfs — very low mass stars and brown dwarfs with spectral types M7 or later (Kirkpatrick et al. 1999; Martín et al. 1999) — are substantially different than those of their higher-mass brethren. Their X-ray and H $\alpha$  emission drop precipitously with temperature (Gizis et al. 2000; West

et al. 2004; Stelzer et al. 2006; Berger et al. 2010), so that ratios of their radio and X-ray luminosities significantly exceed standard relations for active stars (Güdel & Benz 1993; Berger et al. 2001; Williams et al. 2014); a new phenomenology of periodic, highly polarized radio bursts arises (Berger et al. 2005, 2009; Hallinan et al. 2006, 2008); trends relating rotation and X-ray activity break down (Berger et al. 2008; Cook et al. 2014); and their activity lifetimes become much longer than those of Sun-like stars, implying inefficient angular momentum loss and rapid rotation even to  $\sim$ Gyr ages (Gizis et al. 2002; West et al. 2008; Bouvier et al. 2014).

Route & Wolszczan (2016) discovered that the T6 WISEP J112254.73+255021.5 (hereafter WISE 1122+25) is one of the handful of known radio-emitting T dwarfs (Route & Wolszczan 2012; Williams et al. 2013; Kao et al. 2016) in the course of a large Arecibo survey for radio bursts from ultracool dwarfs at 5 GHz (Route & Wolszczan 2013). Along with being an extreme object in terms of its temperature, Route & Wolszczan (2016) claimed that it is extreme in terms of rotation: they phased the arrival time of its radio bursts (Section 2) to infer a rotation period of  $\sim 17.3$  minutes. If confirmed, this rotation period would be by far the shortest ever measured in a brown dwarf. WISE 1122+25 may therefore be a unique laboratory for understanding the relationship between age, rotation, and magnetic field generation in the fully-convective dynamo regime.

The outline of this paper is as follows. We first summarize previous observations of WISE 1122+25 (Section 2). We then describe new follow-up observations that we obtained with the Karl G. Jansky Very Large Array (VLA) and Gemini-North and present the data (Section 3). Next we analyze

the data for periodic signals, finding evidence for variations at a period of  $\sim 116$  min rather than the value suggested by Route & Wolszczan (2016), and analyze the properties of the observed radio emission (Section 5). Finally, we discuss the implications of these results (Section 6) and present our conclusions (Section 7).

## 2. THE RADIO-ACTIVE T6 DWARF WISEP J112254.73+255021.5

Kirkpatrick et al. (2011) identified WISE 1122+25 as a candidate T dwarf in *Widefield Infrared Survey Explorer* (WISE) imaging and confirmed its cool nature spectroscopically, assigning it a NIR spectral type of T6. Additional analysis has yielded a spectrophotometrically estimated distance of 17.7 pc (Kirkpatrick et al. 2012).

Over a span of four observing epochs in their 5 GHz Arecibo survey, Route & Wolszczan (2013, 2016) detected five radio bursts from WISE 1122+25. The peak fluxes were  $\sim 1.5$ – $3$  mJy, and two of the bursts were separated by  $\sim 18.3$  minutes. In ten additional, non-contiguous hours of follow-up observations, additional flares were not detected; the total time on source was 29 hr. The detected flares had left circular polarization (LCP) fractions ranging from 15–100% and characteristic durations of 30–120 s. Route & Wolszczan (2016) did not find a quiescent counterpart to the radio source in the FIRST catalog of radio sources (Becker et al. 1995).

The high circular polarization fraction and brightness temperature of WISE 1122+25’s radio bursts are consistent with emission due to the electron cyclotron maser instability (ECMI; Wu & Lee 1979; Treumann 2006), as also observed in a substantial fraction of the radio-active ultracool dwarfs (Burgasser & Putman 2005; Hallinan et al. 2006, 2008; Berger et al. 2009; Route & Wolszczan 2012; Williams & Berger 2015). Because this emission is expected to occur at the local electron cyclotron frequency,  $\nu_c = eB/2\pi m_e c \simeq 2.8 \text{ GHz}(B/\text{kG})$ , radio detection provides a measurement of the magnetic field strength at the site of the radio emission. In the case of WISE 1122+25, Route & Wolszczan (2016) estimated  $B \gtrsim 1.8$  kG since the upper spectral cutoff was not observed.

Route & Wolszczan (2016) also applied pulsar timing techniques to search for a periodicity in the times-of-arrival (TOAs) of WISE 1122+25’s flares. They obtained a timing solution of  $P = 1035.7881 \pm 0.0008 \text{ s} \simeq 17.3$  minutes, with a post-fit rms residual  $\sigma \approx 0.86$  s, although they emphasize that these uncertainties are the formal outputs of the fitting routine and that the variability in the flare profiles suggests that the true uncertainty in the period is  $\sim 15$  s: a number that is substantially larger but still small in an absolute sense. The first and last flare detections were separated by  $\sim 240$  days, or  $\sim 20,000$  rotations assuming the claimed periodicity. Route & Wolszczan (2016) used Monte Carlo simulation to deduce a false-alarm probability of  $\sim 0.01\%$  for the period detection. This ultra-short rotation period implies a highly oblate object rotating near its breakup rate, with an equatorial velocity

$\gtrsim 300 \text{ km s}^{-1}$  (Route & Wolszczan 2016). The breakup rotation rate is a function of mean density, which increases with time in the brown dwarf regime, so that the observed period implies an age  $\gtrsim 1$  Gyr for WISE 1122+25 (Route & Wolszczan 2016). Other constraints on the age of WISE 1122+25 are not presently available.

The M5 dwarf LHS 302 is found  $\sim 4.4'$  away from WISE 1122+25 and appears to have a similar distance and proper motion. If the two objects were physically related, their projected separation would be  $\sim 4500$  AU, so that interactions between the two would be expected to be negligible (Kirkpatrick et al. 2011).

## 3. OBSERVATIONS AND DATA PROCESSING

### 3.1. Karl G. Jansky Very Large Array

We obtained Director’s Discretionary time to observe WISE 1122+25 for 3 hours using the VLA on UT date 2016 May 11 (project ID VLA/16A-463; PI: Williams). The VLA was in the semi-extended “CnB” configuration. We used the VLA’s 3-bit samplers to digitize the full bandwidth of the “C” band, 4–8 GHz, dividing the bandpass into channels of 2 MHz width. We obtained standard calibration observations, using 3C 286 as the flux density and bandpass calibrator and NVSS J112555+260630 as the complex gain calibrator. The total time on-source was 2.57 hr.

We used standard procedures to analyze the data, using a Python-based reduction process driving tasks from the CASA package (McMullin et al. 2007). We flagged radio-frequency interference (RFI) automatically using the morphological and SumThreshold algorithms as implemented by the aoflagger tool (Offringa et al. 2010, 2012). After calibration, we imaged the total intensity (Stokes I polarization component) of the full data set at  $0.3 \times 0.3 \text{ arcsec}^2$  resolution using multifrequency synthesis (Sault & Wieringa 1994) and  $w$ -projection (Cornwell et al. 2005). The mean frequency of this image is 6.00 GHz and the rms noise around its phase center is  $2.2 \mu\text{Jy bm}^{-1}$ .

The image contains an isolated source at position RA = 11:22:54.26, Decl. = +25:50:20.0, with uncertainties of  $0.2''$  and  $0.1''$  in RA and Decl., respectively. From the astrometric parameters reported by Kirkpatrick et al. (2011) and the mean image epoch of MJD 57519.27, the predicted position of WISE 1122+25 at the time of our observation is RA = 11:22:54.30, Decl. = +25:50:20.4, with uncertainties of  $0.5''$  and  $0.6''$  in RA and Decl., respectively. These two positions differ by  $0.7''$  or  $1.3\sigma$ . Based on this agreement and the time-variable polarized emission of this source (described below), which is characteristic of radio-active ultracool dwarfs, we identify this VLA source with WISE 1122+25.

We generated two additional images by splitting the 4 GHz of VLA bandwidth into halves by frequency, resulting in two images with center frequencies of 5.00 and 7.00 GHz. In the low-band image, WISE 1122+25 is a point source with a

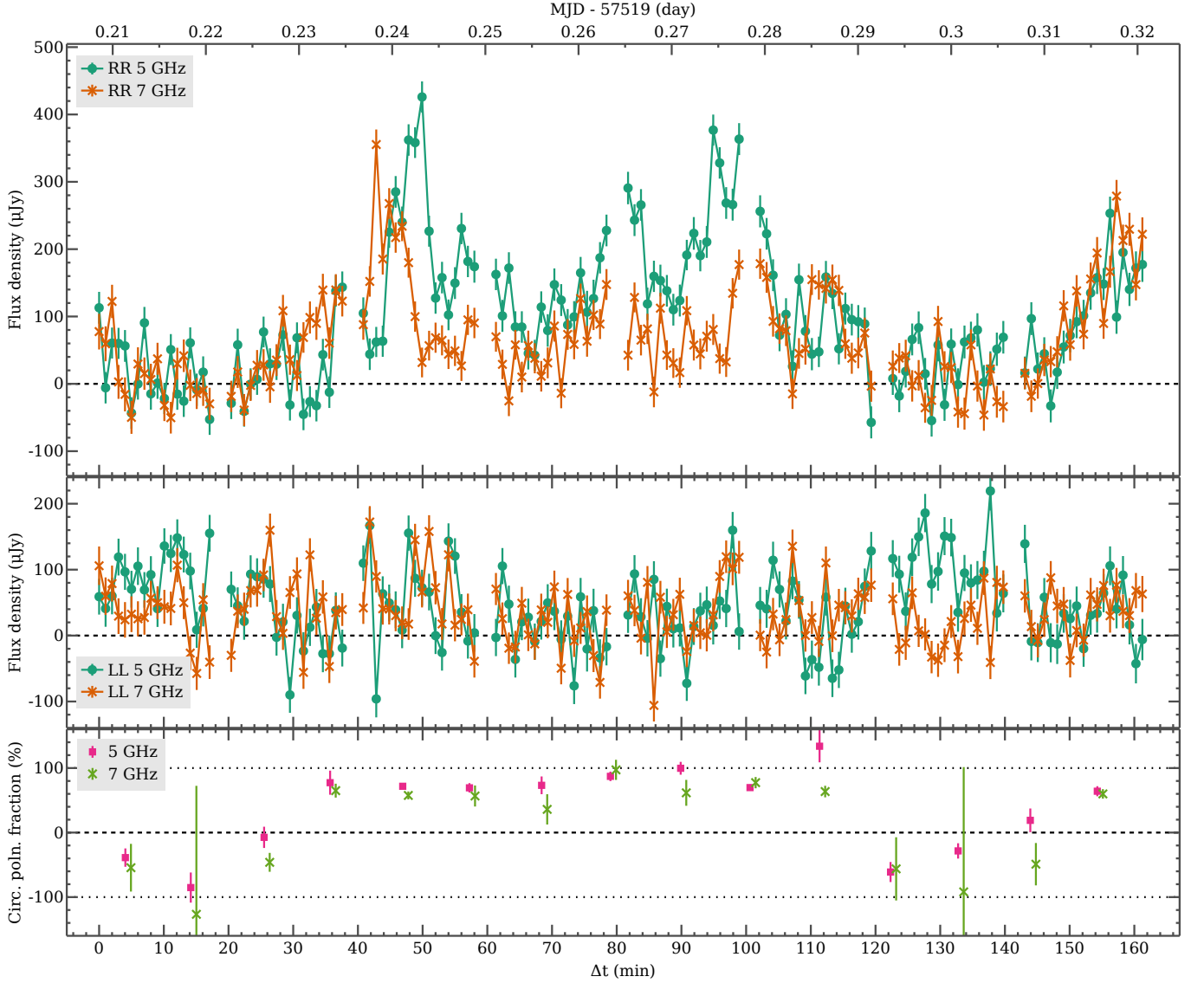


**Figure 1.** Radio light curves of [WISE 1122+25](#) from the VLA, binned to a 1-minute cadence from the 10 s cadence at which the visibilities were averaged. The total duration of the observations is 162 minutes. *Top panel:* light curves in the RR polarization product. *middle panel:* light curves in the LL polarization product. *Green circles:* data in the 4–6 GHz sub-band. *Orange X's:* data in the 6–8 GHz sub-band. Breaks in the lines indicate pauses in the observations for calibrator visits. *Bottom panel:* derived circular polarization fraction in the 4–6 GHz sub-band, after Hanning smoothing the RR and LL data to 10-minute time scales. Full RCP is +100% and full LCP is −100%. Data at the two frequencies are slightly offset in time for visual clarity.

time- and polarization- averaged flux density of  $77 \pm 4 \mu\text{Jy}$ . In the high-band image, it is a point source with an averaged flux density of  $47 \pm 4 \mu\text{Jy}$ . The implied spectral index, averaging over time and polarization, is  $\alpha = -1.5 \pm 0.3$ , where  $S_\nu \propto \nu^\alpha$ .

We investigated the time variability of [WISE 1122+25](#) by subtracting the emission from the other sources in the VLA field of view and summing the calibrated visibilities after phasing to the source position, as per the procedure described in Williams et al. (2013). Light curves derived from this analysis are shown in Figure 1, where curves have been binned to a cadence of 60 s (compared to the data sampling time of 5 s) for display purposes. Here and below we quantify

times using  $\Delta t$ , the number of minutes since the observation start;  $\Delta t = 0$  is MJD = 57519.208.

The emission in the RR polarization product (that is, the mean correlation of pairs of RCP-sensitive receivers) is highly variable, with several bursts, predominantly in the 4–6 GHz sub-band (denoted “5 GHz” for brevity), having durations of  $\sim 10$  min and peak flux densities of  $\sim 300$ – $400 \mu\text{Jy}$ . The second and third 5 GHz RR bursts are separated by  $\sim 16$  minutes, close to the  $\sim 18.3$  minute spacing between the two closest Arecibo bursts. This separation in turn presumably drove the identification of a  $\sim 17.3$ -minute periodicity by Route & Wolszczan (2016). We note, however, that the Arecibo bursts were LCP rather than RCP.

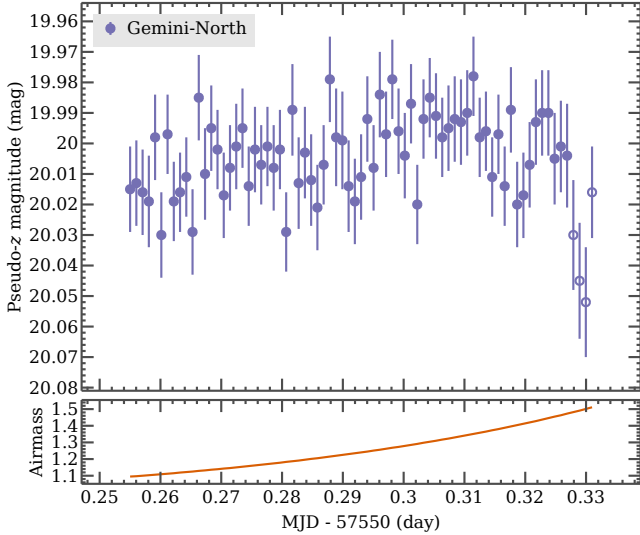


**Figure 2.** Red optical light curve of **WISE 1122+25** from Gemini-North. Un-filled circles indicate observations made at high airmass ( $z > 1.48$ ) not included in subsequent analysis. The sample cadence is 133 s and the total duration of the observation (including the high-airmass points) is 109 minutes.

The RR emission is generally brighter in the 5 GHz sub-band than the 7 GHz sub-band, with the exception of the period  $30 \lesssim \Delta t \lesssim 45$ , which ends in a rapid spike. Finer-grained examination of the frequency dependence of the emission does not reveal any abrupt changes in the spectrum. If there is a sharp spectral cutoff as expected from the ECMI emission, it occurs at higher frequencies than we observed.

While the LL polarization product is not as clearly variable, there are two episodes in which the LL emission at 5 GHz becomes significantly brighter than that at 6–8 GHz (“7 GHz”): at  $\Delta t \sim 5$  and  $\Delta t \sim 130$ . These episodes coincide with periods of weak or absent emission in the RR polarization product, so that at most times the radio emission of **WISE 1122+25** is strongly circularly polarized, although the handedness of that polarization varies. The lower panel of **Figure 1** plots the polarization fraction as a function of time, smoothing on 10-minute time scales to increase S/N. The emission is almost always intensely circularly polarized, with only a few intervals where the absolute value of the polarization fraction is  $< 50\%$ . These intervals seem to correspond to transitions in the handedness of the polarization, from left to right and back again.

The Arecibo flares were 15–100% LCP, had durations of  $\sim 1$ –3 min, and reached peak flux densities of 1000–2000  $\mu\text{Jy}$  (Route & Wolszczan 2016). The dominant RR radio variability that we observe is therefore substantially different in its gross properties. The episodes of LL emission, however, could represent higher-frequency and fainter counterparts of the Arecibo flares. Using the spectral index derived above, the Arecibo flares would have flux densities  $\sim 1$ –2 mJy, significantly brighter than the LCP emission we observed.

### 3.2. Gemini-North

We observed **WISE 1122+25** on UT date 2016 June 21 with the Gemini Multi-Object Spectrograph (GMOS-N; Hook et al. 2004) on the Gemini-North Telescope (Program GN-2016A-FT-29) in imaging mode. We used the  $z$  (G0304) filter with the e2v deep depletion detectors. The  $z$ -band blue edge of 850 nm is set by the filter, but the red cutoff is set by the detector which extends to 950–1000 nm, approximately 100 nm redder than most CCD detectors.

The data were taken over 1.8 hr and consist of 75 images with 60 s exposure times. The observations began after the object had already transited the meridian and spanned an airmass of 1.1 to 1.5. We processed the data in the standard way using the Gemini IRAF package. We corrected fringing using the observatory’s fringe image and measured aperture photometry for the target relative to the average of five comparison stars in the field of view to remove the first-order effects of seeing and airmass variations. **Figure 2** shows the resulting light curve. We do not include in our analysis the final four images made at airmass  $z > 1.48$ . Calibrating from the SDSS photometry for these comparison stars yields  $z = 20.00$  mag for **WISE 1122+25**. The observed scatter for **WISE 1122+25**,  $\pm 0.014$  mag, is consistent with the expected noise due to photon counting statistics. We rule out sinusoidal peak-to-peak amplitudes  $\gtrsim 1.5\%$  for periods less than one hour.

## 4. PERIODICITY ANALYSIS

While **Figure 2** shows no clear evidence for a periodicity in the Gemini-North data, the peaks in the VLA light curve (**Figure 1**) suggest a possible periodic signal. We investigated this possibility using a phase dispersion minimization analysis (PDM; Stellingwerf 1978). In this technique, given a trial period  $P$ , the data are placed into phase bins and the overall scatter within each bin is summarized with a statistic denoted  $\Theta$ . Lower values of  $\Theta$  imply less scatter and therefore a better phasing. Unlike some other periodicity-finding techniques (e.g., the Lomb-Scargle periodogram; Lomb 1976; Scargle 1982), PDM analysis therefore makes no assumptions about the underlying structure of the potential periodic signal. In this work we used the implementation of PDM provided by version 0.8.4 of the **pwkit** Python toolkit<sup>1</sup>.

**Figure 3** plots  $\Theta(P)$  in the VLA and Gemini-North data sets, where we subdivided the VLA data by polarization and frequency sub-band. The periods range from one minute to just below the respective durations of the observations. The PDM analysis does not reveal evidence of a periodic signal in the Gemini-North data. The VLA RR data, on the other hand, show clear but broad minima at periods of  $\sim 55$  and  $\sim 116$  minutes. The LL data show weak evidence for similar periodicities. Three out of the four VLA  $\Theta$  curves have their

<sup>1</sup> <https://github.com/pkgw/pwkit/>



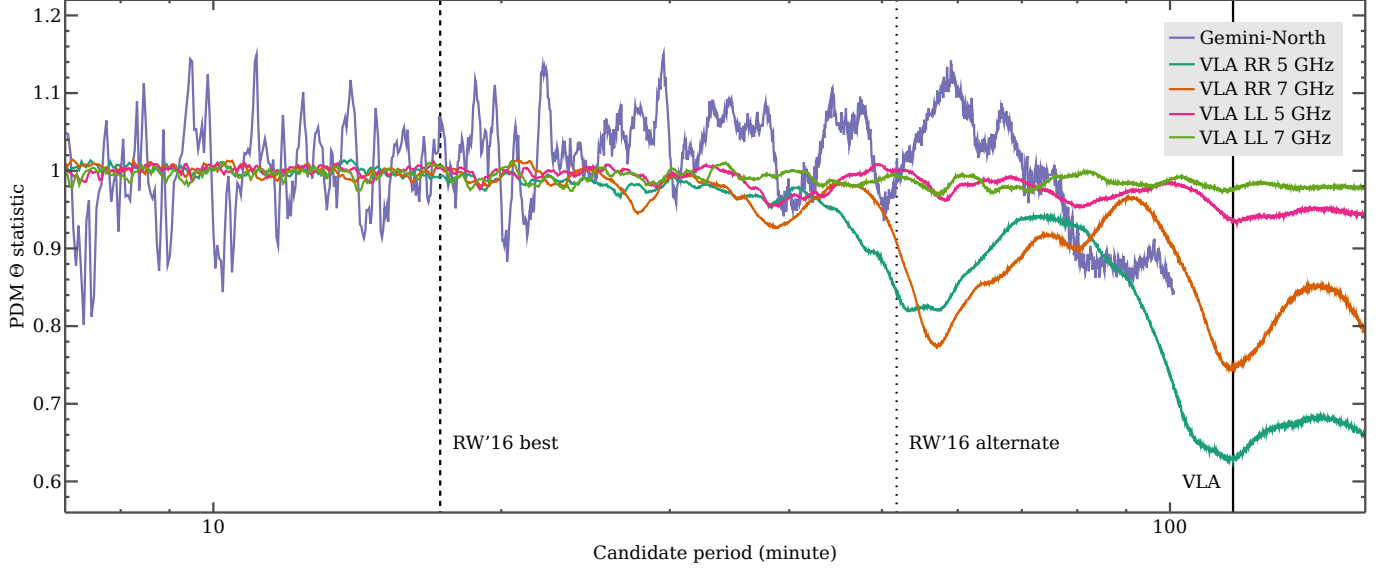


**Figure 3.** Phase dispersion minimization (PDM) statistic  $\Theta$  for trial phasings of the VLA and Gemini-North data sets. While there is no clear periodicity in the Gemini-North data, the VLA data show multiple minima suggesting plausible phasings. *Vertical solid line* shows the best phasing of the VLA LL 5 GHz data set, which is also the close to the best phasings of the LL 7 GHz and RR 5 GHz light curves. *Vertical dashed line* shows the periodicity  $P = 17.26$  min suggested by Route & Wolszczan (2016). Our data do not show evidence for periodic variability at this value. *Vertical dotted line* shows another candidate periodicity,  $P = 51.79$  min, reported by those authors.

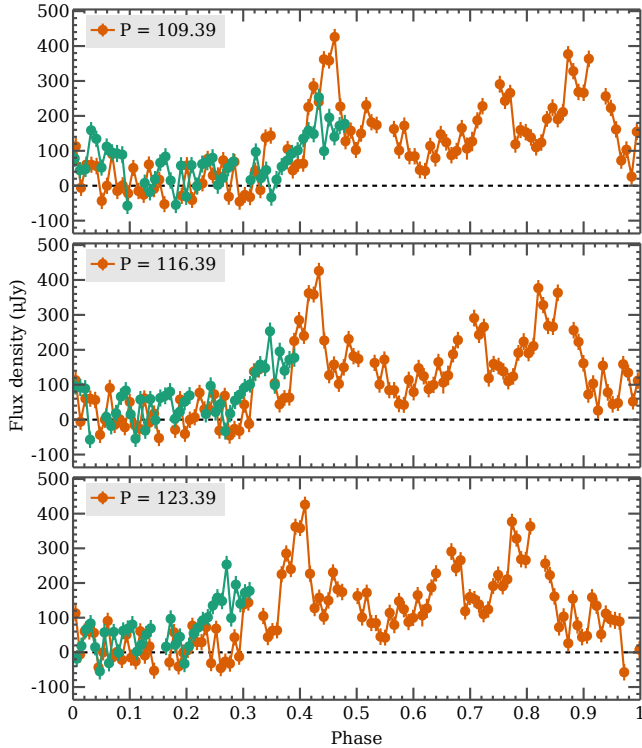


**Figure 4.** The VLA RR 5 GHz light curve phased at different candidate periodicities. Different colors represent different successive rotations.

global minimum near the larger of these periodicities. We note that the four curves are derived from data that are statistically independent in principle. A time-dependent calibration error could induce correlations between the different polarization and frequency groupings, but PDM analysis of a nearby

reference source shows no indications of such an effect.

Inspection of Figure 1 shows that the smaller period minimum represents an approximate phasing of the three peaks seen in the VLA RR 5 GHz data at  $\Delta t = 50, 100$ , and 160, while the larger is approximately its first sub-harmonic, aligning the first and third of these peaks as well as the troughs of  $\sim$ zero RR emission before them. Assuming the shorter (longer) candidate period, our VLA observation spanned 2.9 (1.4) cycles of emission. Although the longer candidate period result is therefore associated with substantially worse phase coverage, with only 0.4 of a period having any redundant data, the scatter at that phasing is lower than that at the shorter period, as reflected by the fact that it indeed corresponds to the global minimum of the PDM  $\Theta$  statistic computed for this data set. We proceed under the assumption that the longer candidate periodicity corresponds to the rotation period of WISE 1122+25.

A Monte Carlo assessment of the uncertainty on this periodicity, computed by adding noise to the observed data and re-running the PDM analysis, suggests an uncertainty of 0.7 min. This value, however, understates the true uncertainty given the limited available data. In Figure 4 we plot the VLA RR 5 GHz data phased at our preferred periodicity and two periods offset from the PDM-minimized value by  $\pm 7$  minutes. These phasings are visibly inferior to the PDM-optimized value but do not appear implausible. Assuming the emission is indeed periodic, we suggest that a plausible uncertainty on our measurement is about this large.

If the Arecibo radio bursts occur at the same periodicity as the VLA variability, the flare TOAs reported by Route & Wolszczan (2016) could potentially yield a more precise con-

straint on [WISE 1122+25](#)’s periodicity. To investigate this, we examined possible TOA phasings at periods between 106 and 126 minutes. The five burst TOAs reported by Route & Wolszczan (2016) span three primary time scales: the gap between the first and second TOA is  $\sim 230$  days; the gap between the second and third is  $\sim 18$  minutes; and the gaps between the third, fourth, and fifth TOAs are  $\sim 4$  days each. There are therefore reasonable grounds to argue that the first TOA should not be included in a timing solution, since it is so distant from the others, and/or that the second or third TOA should not be included, since their separation is small compared to the VLA light curve period. Regardless of which, if any, TOAs we discard from the analysis, no preferred periodicity emerges within the general bounds supported by the VLA light curve.

### 5. ANALYSIS OF THE RADIO EMISSION

The variability of [WISE 1122+25](#) makes it difficult to assess the brightness of its quiescent radio emission. The mean flux densities during the troughs of RR emission,  $6 < \Delta t < 24$  and  $121 < \Delta t < 147$ , are almost all consistent with zero. The exception is the 5 GHz sub-band in the second trough, where the mean flux density is  $33.7 \pm 5.0 \mu\text{Jy}$ . Comparing to the LL emission at these times, this elevated RR emission is likely related to the relatively bright, low-band LL burst that occurs at this time. The mean 5 GHz LL flux density in this window is  $95 \pm 6 \mu\text{Jy}$ , implying a  $\sim 50\%$  LCP flare of total intensity  $I = \text{LL} + \text{RR} = 130 \pm 8 \mu\text{Jy}$ . This polarization fraction is consistent with the Arecibo events, but the flux density is an order of magnitude lower (Route & Wolszczan 2016).

The mean LL flux densities of [WISE 1122+25](#) in the window centered between the two RR flares,  $60 < \Delta t < 96$ , are  $18 \pm 5$  and  $13 \pm 4 \mu\text{Jy}$  in the 5 and 7 GHz sub-bands, respectively. We did not obtain the calibrator observations necessary to calibrate the leakage between the VLA’s RR and LL receivers in our observation, so that the LL correlations will include a small contribution of RR flux, and vice versa. This is typically a 5% effect, whereas the observed LL flux density during this short period represents  $(11 \pm 3)\%$  of the RR flux density. We therefore cannot exclude that the measured LL flux density in this time window is entirely due to leakage from the RR emission.

The data suggest that RR and LL components of the radio emission of [WISE 1122+25](#) both vary periodically (Figure 3), but  $180^\circ$  out of phase, with their respective maxima including strongly polarized flares lasting  $\sim 15$  minutes and their minima consistent with zero emission. Therefore, while the mean flux density of [WISE 1122+25](#) in our observation results in an easy VLA detection ( $64 \pm 3 \mu\text{Jy}$  at 6 GHz with a spectral index  $\alpha = -1.5 \pm 0.3$ ), this T dwarf may have *no* quiescent emission, defining this to mean a non-variable, broadband component. High-sensitivity radio observations with full polarimetric calibration are needed to confirm this. The radio

flares detected by Arecibo are  $\gtrsim 200$  times brighter than the quiescent component, taking the brightness of the latter to be  $\lesssim 10 \mu\text{Jy}$ . This ratio is comparable to the extreme values found in [2M 1047+21](#) (Williams et al. 2013) and the M8 dwarf [DENIS J1048.0–3956](#) (Burgasser & Putman 2005).

While [WISE 1122+25](#) may not produce “quiescent” radio emission as defined above, its time-averaged radio flux density is relevant to the overall energetics of the nonthermal particle acceleration processes that power its radio emission. Assuming a 20% uncertainty on its estimated 17.7 pc distance, we compute  $\langle L_{\nu, R} \rangle = 10^{13.4 \pm 0.2} \text{ erg s}^{-1} \text{ Hz}^{-1}$  at 6 GHz. This is typical of radio-active ultracool dwarfs (Williams et al. 2014). Using the polynomial relationship between spectral type and  $L_{\text{bol}}$  developed by Filippazzo et al. (2015), we estimate the bolometric luminosity to be  $10^{-4.89 \pm 0.13} L_\odot$ , and therefore that in a time-averaged sense,  $\langle L_{\nu, R} \rangle / L_{\text{bol}} = 10^{-15.4 \pm 0.2} \text{ Hz}^{-1}$ . This is the highest value yet measured for an ultracool dwarf (Williams et al. 2014; Williams & Berger 2015), a result driven by the late spectral type of [WISE 1122+25](#); as shown by Filippazzo et al. (2015), the bolometric luminosities of brown dwarfs are believed to decrease rapidly as a function of spectral type for objects later than  $\sim T3$ . That being said, we calculate that both of the two other late T dwarfs detected at radio wavelengths, [2M 1047+21](#) and [2MASS J12373919+6526148](#), are half as radio-bright as [WISE 1122+25](#) by this metric, having  $\langle L_{\nu, R} \rangle / L_{\text{bol}} \sim 10^{-15.7} \text{ Hz}^{-1}$  (Williams & Berger 2015; Kao et al. 2016).

Route & Wolszczan (2016) interpreted the Arecibo radio bursts as being due to the ECMI, which results in bursty, highly-polarized emission with brightness temperatures that can significantly exceed the canonical limit of  $10^{12}$  K associated with the inverse Compton catastrophe (Kellermann & Pauliny-Toth 1969). The non-bursting radio emission from ultracool dwarfs is often argued to instead originate from gyrosynchrotron processes (e.g., Berger 2002), which results in steadier, less polarized emission with typically observed brightness temperatures of  $\sim 10^{8-10}$  K (e.g., Osten et al. 2006). Assuming the characteristic length scale of the emitting region to be  $R_J$ , we place a conservative lower limit on the brightness temperature of the VLA emission to be  $T_b \gtrsim 10^{9.2}$  K, consistent with gyrosynchrotron. Route & Wolszczan (2016) obtain a higher limit,  $4 \times 10^{11}$  K, for the Arecibo bursts, which are brighter and more probably originate from a compact emission region. However, while gyrosynchrotron emission can in principle be highly circularly polarized (Dulk 1985), this requires specialized circumstances that are difficult to achieve in practice. ECMI or perhaps plasma emission is therefore the more likely origin of the emission that we observed with the VLA. Observations at higher frequencies could potentially discriminate between these possibilities because the spectrum of ECMI emission cuts off strongly at frequencies above the local electron cyclotron frequency  $\nu_c = eB/2\pi m_e c \approx 2.8(B/\text{kG}) \text{ GHz}$ , while gyrosynchrotron

emission is spectrally smooth. Under the ECMI model, we can place a somewhat higher limit on the magnetic field strength of [WISE 1122+25](#) than [Route & Wolszczan \(2016\)](#) because our observations extended to higher frequencies. If the rapid event in the 7 GHz sub-band at  $\Delta t \sim 43$  is due to ECMI, the magnetic field of [WISE 1122+25](#) must reach strengths of  $B \gtrsim 2.5$  kG.

## 6. DISCUSSION

We have discovered evidence for variations in the radio emission of [WISE 1122+25](#) with a tentative period of  $\sim 116$  min. The features that drive this periodicity are the deep troughs in the RR emission, the rising slopes that follow them, and weaker, low-frequency LL emission features at  $\Delta t \sim 5$  and 130. Because our VLA observation lasted only 162 min, yielding overlapped phase coverage of only 0.4 of a rotation, the periodicity we detect should be regarded as provisional. We also see no compelling signs of variability at any periodicity in the Gemini-North data, although our observations did not last as long as this candidate periodicity. Regardless of the VLA periodicity's validity, however, we do not find evidence for periodic variability in the radio or red optical emission of [WISE 1122+25](#) at the period of  $17.26313 \pm 0.00001$  min proposed by [Route & Wolszczan \(2016\)](#).

If the true rotation period of [WISE 1122+25](#) is 116 min rather than 17 min, it is not nearly as extreme of an object as initially proposed ([Route & Wolszczan 2016](#)). In fact, it then becomes a slightly slower rotator than [2M 1047+21](#), the only other T dwarf to have its rotation period derived from its radio emission ([Williams & Berger 2015](#)), which has  $P \approx 106$  min. Assuming a radius of  $0.9 \pm 0.15 R_J$  for [WISE 1122+25](#), the same as [2M 1047+21](#) ([Vrba et al. 2004](#); [Williams & Berger 2015](#)), we find an equatorial rotational velocity of  $\sim 60 \text{ km s}^{-1}$  for [WISE 1122+25](#).

In these data the radio emission of [WISE 1122+25](#) is strongly circularly polarized, but the handedness of the polarization changes twice. If this change in handedness is confirmed to occur periodically, this would be consistent with a model in which the magnetosphere of [WISE 1122+25](#) is a dipole tilted with respect to its rotation axis, as proposed by [McLean et al. \(2011\)](#) to explain VLA observations of the extremely radio-active, benchmark M7 binary [NLTT 33370 AB](#) (= 2MASS J13142039+1320011; see also [Schlieder et al. 2014](#); [Williams et al. 2015](#); [Forbrich et al. 2016](#); [Dupuy et al. 2016](#)). We show a schematic of the proposed model in [Figure 5](#). Each pole produces highly circularly polarized radio emission, with the oppositely-aligned polar magnetic fields leading to opposite handedness of the resulting emission. The significantly brighter emission in the RR polarization mode suggests that the magnetic north pole (i.e., analogous to Earth's geographic south pole) is more directly pointed towards Earth ([Kaiser et al. 1978a,b](#)). Assuming that the intrinsic radio emission of each magnetic pole is approximately the same, the shapes of the observed light curves in each

polarization could be used to constrain the inclination  $i$  of the rotation axis of [WISE 1122+25](#) and the angle  $\theta$  between this axis and the magnetic dipole axis: for instance,  $i = 90^\circ$  and  $\theta = 0^\circ$  leads to a non-variable, unpolarized light curve; while  $i = \theta = 0^\circ$  leads to a non-variable, 100% polarized light curve; and  $i = 0^\circ$ ,  $\theta = 90^\circ$  leads to out-of-phase curves of 100% circular polarization, as observed here. We therefore speculate that the magnetic dipole axis of [WISE 1122+25](#) may be highly misaligned with its rotation axis.

The lack of observed  $z$ -band variability in [WISE 1122+25](#) can only rule out relatively short ( $\lesssim 1$  hr) periods with relatively high ( $\gtrsim 1.5\%$ ) amplitudes. [Metchev et al. \(2015\)](#) found that 36% of T dwarfs vary in the mid-infrared Spitzer bands at  $>0.4\%$ . [Radigan et al. \(2014\)](#) argue that at J band, sinusoidal amplitudes larger than 2% are found only for L/T transition objects (spectral types L9–T3.5), but that 80% of other L/T dwarfs vary at the 0.5%–1.6% level. [Heinze et al. \(2015\)](#) argued that for T dwarfs, variability in the red optical (F814W, 700–950 nm) has a higher amplitude than at J band or Spitzer bands. Given these statistics, [WISE 1122+25](#) cannot be viewed as an outlier. However, [Kao et al. \(2016\)](#) argue for a possible correlation between radio activity and the presence of optical and infrared variability which they attribute to aurorae. In this aurora model, the lack of red-optical variability may be more surprising.

## 7. CONCLUSIONS

[WISE 1122+25](#) is the fourth T dwarf with a published detection at radio wavelengths ([Route & Wolszczan 2012, 2016](#); [Williams et al. 2013](#); [Kao et al. 2016](#)). While early theoretical work motivated a consensus that the magnetic fields of such cool objects should be negligible (*e.g.*, [Durney et al. 1993](#)), radio surveys have demonstrated that in fact  $\sim 10\%$  of these objects host both organized, kG-strength magnetic fields and the nonthermal particle acceleration processes necessary to drive radio emission ([Route & Wolszczan 2013, 2016](#); [Kao et al. 2016](#)). It remains unknown what fraction of the remaining objects do not possess strong, organized fields at all, and what fraction possess such fields but not the acceleration processes necessary to render them detectable via radio emission.

While the bursts from [WISE 1122+25](#) detected by [Route & Wolszczan \(2016\)](#) are similar to the bright, highly polarized ECMI bursts detected from a growing list of ultracool dwarfs, the emission we have detected with the VLA is unique in that it has both a high duty cycle and strong circular polarization of alternating handedness. For instance, while the handedness of the circularly polarized emission from [NLTT 33370 AB](#) also oscillates, it is accompanied by a much more prominent unpolarized component as well ([McLean et al. 2011](#); [Williams et al. 2015](#)). We have speculated that the particular variability pattern we have observed may be due to a magnetic dipole axis that is highly misaligned with respect to the object's rotation axis ([Figure 5](#)). The lack of unpolarized emission may also imply that [WISE 1122+25](#) does not possess equatorial belts

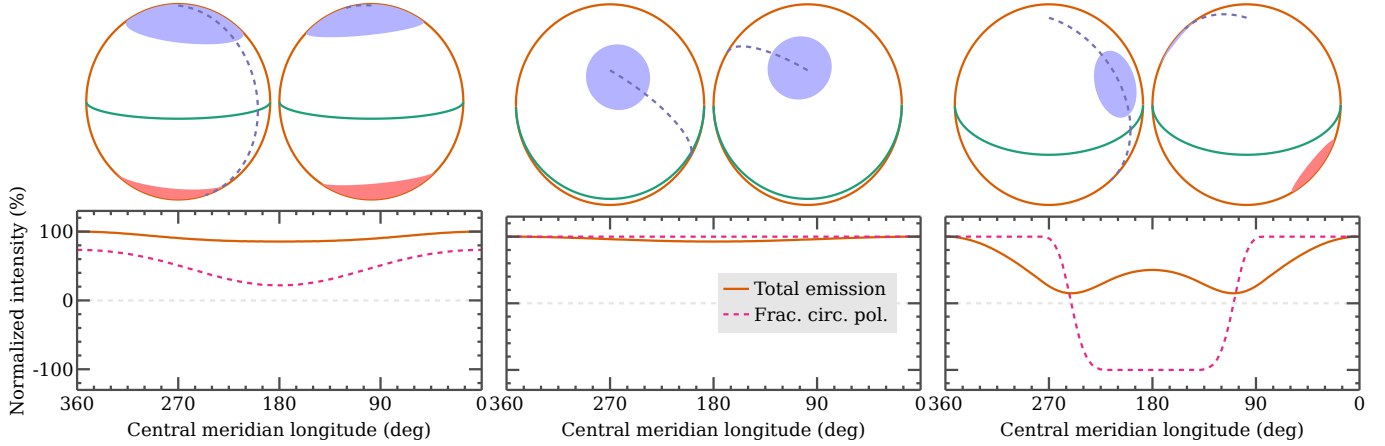


**Figure 5.** A schematic for interpreting the intensity/polarization light curve of [WISE 1122+25](#). Upper row: orthographic projections of brown dwarf configurations. Solid green line is the equator, blue is RR-emitting magnetic dipolar cap, red is LL-emitting magnetic dipolar cap, and dashed line is zero longitude, defined to intersect both the rotational and magnetic poles. Each pair of projections shows the object at central meridian longitude CML = 300° and CML = 120°. The longitude system is planetocentric (see, e.g., [Zangari 2015](#)), so that CML decreases with time. Lower row: light curves of total intensity (RR + LL; orange solid) and fractional circular polarization ((RR - LL)/(RR + LL); purple dashed) over one rotation, assuming isotropic emission. Total intensity is normalized to its maximum. Left column: configuration with inclination  $i = 80^\circ$ , dipole offset  $\theta = 6^\circ$ , cap radius  $\phi = 40^\circ$ . Middle column:  $i = 20^\circ$ ,  $\theta = 6^\circ$ ,  $\phi = 20^\circ$ . Right column:  $i = 30^\circ$ ,  $\theta = 60^\circ$ ,  $\phi = 20^\circ$ . This resembles the data in [Figure 1](#).

of nonthermal plasma as have been hypothesized to surround [NLTT 33370 AB](#) and other ultracool dwarfs ([Williams et al. 2014, 2015](#)).

Like [2M 1047+21](#), [WISE 1122+25](#) was discovered to be a radio emitter with Arecibo, then followed up with VLA observations ([Route & Wolszczan 2012](#); [Williams et al. 2013](#)). In both cases, the interferometric data revealed details of its radio emission that are inaccessible to Arecibo due to the latter telescope’s confusion limitations and inability to track sources for long ( $\gtrsim 3$  hr) durations. Together, these two complementary, world-class observatories are leading the way in gaining observational insight into the magnetic fields and dynamos of ultra-cool bodies that are nearing the (exo)planetary mass regime.

*Acknowledgments.* The VLA is operated by the National Radio Astronomy Observatory, a facility of the National Sci-

ence Foundation operated under cooperative agreement by Associated Universities, Inc. Based on observations obtained at the Gemini Observatory processed using the Gemini IRAF package, which is operated by the Association of Universities for Research in Astronomy, Inc., under a cooperative agreement with the NSF on behalf of the Gemini partnership: the National Science Foundation (United States), the National Research Council (Canada), CONICYT (Chile), Ministerio de Ciencia, Tecnología e Innovación Productiva (Argentina), and Ministério da Ciência, Tecnologia e Inovação (Brazil). This work made use of NASA’s Astrophysics Data System and the SIMBAD database, operated at CDS, Strasbourg, France.

*Facilities:* Gemini-North, Karl G. Jansky Very Large Array

*Software:* aoflagger, CASA, Gemini IRAF, pwkit

## REFERENCES

- Becker, R. H., White, R. L., & Helfand, D. J. 1995, [ApJ](#), **450**, 559
- Berger, E. 2002, [ApJ](#), **572**, 503
- Berger, E., Ball, S., Becker, K. M., et al. 2001, [Natur](#), **410**, 338
- Berger, E., Rutledge, R. E., Reid, I. N., et al. 2005, [ApJ](#), **627**, 960
- Berger, E., Basri, G., Gizis, J. E., et al. 2008, [ApJ](#), **676**, 1307
- Berger, E., Rutledge, R. E., Phan-Bao, N., et al. 2009, [ApJ](#), **695**, 310
- Berger, E., Basri, G., Fleming, T. A., et al. 2010, [ApJ](#), **709**, 332
- Bouvier, J., Matt, S. P., Mohanty, S., et al. 2014, in *Protostars and Planets VI*, ed. H. Beuther, R. S. Klessen, C. P. Dullemond, & T. Henning (Tucson, AZ, USA: University of Arizona Press), 433
- Burgasser, A. J., & Putman, M. E. 2005, [ApJ](#), **626**, 486
- Cook, B. A., Williams, P. K. G., & Berger, E. 2014, [ApJ](#), **785**, 10
- Cornwell, T. J., Golap, K., & Bhatnagar, S. 2005, in *Astronomical Society of the Pacific Conference Series*, Vol. 347, *Astronomical Data Analysis Software and Systems XIV*, ed. P. Shopbell, M. Britton, & R. Ebert, 86
- Dulk, G. A. 1985, [ARA&A](#), **23**, 169
- Dupuy, T. J., Forbrich, J., Rizzuto, A., et al. 2016, [ApJ in press](#), [arxiv:1605.07182](#)
- Durney, B. R., de Young, D. S., & Roxburgh, I. W. 1993, [SoPh](#), **145**, 207
- Filippazzo, J. C., Rice, E. L., Faherty, J., et al. 2015, [ApJ](#), **810**, 158
- Forbrich, J., Dupuy, T. J., Reid, M. J., et al. 2016, [ApJ in press](#), [arxiv:1605.07177](#)
- Gizis, J. E., Monet, D. G., Reid, I. N., et al. 2000, [AJ](#), **120**, 1085
- Gizis, J. E., Reid, I. N., & Hawley, S. L. 2002, [AJ](#), **123**, 3356
- Güdel, M., & Benz, A. O. 1993, [ApJL](#), **405**, L63
- Hallinan, G., Antonova, A., Doyle, J. G., et al. 2006, [ApJ](#), **653**, 690
- . 2008, [ApJ](#), **684**, 644
- Heinze, A. N., Metchev, S., & Kellogg, K. 2015, [ApJ](#), **801**, 104
- Hook, I. M., Jørgensen, I., Allington-Smith, J. R., et al. 2004, [PASP](#), **116**, 425



- Kaiser, M. L., Alexander, J. K., Riddle, A. C., Pearce, J. B., & Warwick, J. W. 1978a, [GeoRL](#), **5**, 857
- . 1978b, [Geophysical Research Letters](#), **5**, 1087
- Kao, M. M., Hallinan, G., Pineda, J. S., et al. 2016, [ApJ](#), **818**, 24
- Kellermann, K. I., & Pauliny-Toth, I. I. K. 1969, [ApJL](#), **155**, 71
- Kirkpatrick, J. D., Reid, I. N., Liebert, J., et al. 1999, [ApJ](#), **519**, 802
- Kirkpatrick, J. D., Cushing, M. C., Gelino, C. R., et al. 2011, [ApJS](#), **192**, 19
- Kirkpatrick, J. D., Gelino, C. R., Cushing, M. C., et al. 2012, [ApJ](#), **753**, 156
- Lomb, N. R. 1976, [Ap&SS](#), **39**, 447
- Luyten, W. J. 1926, [Harvard College Observatory Bulletin](#), **835**, 2
- Martín, E. L., Delfosse, X., Basri, G., et al. 1999, [AJ](#), **118**, 2466
- McLean, M., Berger, E., Irwin, J., Forbrich, J., & Reiners, A. 2011, [ApJ](#), **741**, 27
- McMullin, J. P., Waters, B., Schiebel, D., Young, W., & Golap, K. 2007, in [Astronomical Society of the Pacific Conference Series](#), Vol. 376, [Astronomical Data Analysis Software and Systems XVI](#), ed. R. A. Shaw, F. Hill, & D. J. Bell, 127
- Metchev, S. A., Heinze, A., Apai, D., et al. 2015, [ApJ](#), **799**, 154
- Offringa, A. R., de Bruyn, A. G., Biehl, M., et al. 2010, [MNRAS](#), **405**, 155
- Offringa, A. R., van de Gronde, J. J., & Roerdink, J. B. T. M. 2012, [A&A](#), **539**, A95
- Ossendrijver, M. 2003, [A&ARv](#), **11**, 287
- Osten, R. A., Hawley, S. L., Bastian, T. S., & Reid, I. N. 2006, [ApJ](#), **637**, 518
- Radigan, J., Lafrenière, D., Jayawardhana, R., & Artigau, E. 2014, [ApJ](#), **793**, 75
- Route, M., & Wolszczan, A. 2012, [ApJL](#), **747**, L22
- . 2013, [ApJ](#), **773**, 18
- . 2016, [ApJL](#), **821**, L21
- Saar, S. H., & Linsky, J. L. 1985, [ApJ](#), **299**, 47
- Sault, R. J., & Wieringa, M. H. 1994, [A&AS](#), **108**, 585
- Scargle, J. D. 1982, [ApJ](#), **263**, 835
- Schatzman, E. 1967, [SoPh](#), **1**, 411
- Schlieder, J., Bonnefoy, M., Herbst, T. M., et al. 2014, [ApJ](#), **783**, 27
- Stellingwerf, R. F. 1978, [ApJ](#), **224**, 953
- Stelzer, B., Micela, G., Flaccomio, E., Neuhäuser, R., & Jayawardhana, R. 2006, [A&A](#), **448**, 293
- Treumann, R. 2006, [A&ARv](#), **13**, 229
- van Maanen, A. 1940, [ApJ](#), **91**, 503
- Vrba, F. J., Henden, A. A., Luginbuhl, C. B., et al. 2004, [AJ](#), **127**, 2948
- West, A. A., Hawley, S. L., Bochanski, J. J., et al. 2008, [AJ](#), **135**, 785
- West, A. A., Hawley, S. L., Walkowicz, L. M., et al. 2004, [AJ](#), **128**, 426
- Williams, P. K. G., & Berger, E. 2015, [ApJ](#), **808**, 189
- Williams, P. K. G., Berger, E., Irwin, J., Berta-Thompson, Z. K., & Charbonneau, D. 2015, [ApJ](#), **799**, 192
- Williams, P. K. G., Berger, E., & Zauderer, B. A. 2013, [ApJL](#), **767**, L30
- Williams, P. K. G., Cook, B. A., & Berger, E. 2014, [ApJ](#), **785**, 9
- Wu, C. S., & Lee, L. C. 1979, [ApJ](#), **230**, 621
- Zangari, A. 2015, [Icarus](#), **245**, 93